Published in final edited form as:
Neuroscience. 2013 January 15; 229: 55–70. doi:10.1016/j.neuroscience.2012.10.069.

Failure of Axonal Transport Induces a Spatially Coincident Increase in Astrocyte BDNF Prior to Synapse Loss in a Central Target

Samuel D. Crish[a,1], **Jason D. Dapper**[a,2], **Sarah E. MacNamee**[a,3], **Pooja Balaram**[a,4], **Tatiana N. Sidorova**[a], **Wendi S. Lambert**[a], and **David J. Calkins**[a,b,§]

Samuel D. Crish: scrish@neoucom.edu; Sarah E. MacNamee: smac3@email.arizona.edu; Pooja Balaram: pooja.balaram@vanderbilt.edu; Tatiana N. Sidorova: tatiana.n.sidorova@vanderbilt.edu; Wendi S. Lambert: wendi.s.lambert@vanderbilt.edu

[a]The Vanderbilt Eye Institute, Vanderbilt University Medical Center, 11425 Langford Medical Research Building IV, 2213 Garland Avenue, Nashville, TN 37232, USA

[b]Vanderbilt Brain Institute, Vanderbilt University Medical Center, U1205 Medical Research Building III, 465 21st. Avenue South, Nashville, TN 37232, USA

Abstract

Failure of anterograde transport to distal targets in the brain is a common feature of neurodegenerative disease. We have demonstrated in rodent models of glaucoma, the most common optic neuropathy, early loss of anterograde transport along the retinal ganglion cell (RGC) projection to the superior colliculus (SC) is retinotopic and followed by a period of persistence of RGC axon terminals and synapses through unknown molecular pathways. Here we using the DBA/2J mouse model of hereditary glaucoma and an acute rat model that retinotopically-focal transport deficits in the SC are accompanied by a spatially coincident increase in brain-derived neurotrophic factor (BDNF), especially in hypertrophic astrocytes. These neurochemical changes occur prior to loss of RGC synapses in the DBA/2J SC. In contrast to BDNF protein, levels of *Bdnf* mRNA decreased with transport failure, even as mRNA encoding synaptic structures remained unchanged. In situ hybridization signal for *Bdnf* mRNA was strongest in SC neurons, and labelling for the immature precursor pro-BDNF was very limited. Subcellular fractionation of SC indicated that membrane-bound BDNF decreased with age in the DBA/2J, while BDNF released from vesicles remained high. These results suggest that in response to diminished axonal function, activated astrocytes in the brain may sequester mature BDNF released from target neurons to counter stressors that otherwise would challenge survival of projection synapses.

Corresponding author: David J. Calkins, The Vanderbilt Eye Institute, Vanderbilt University Medical Center, 11435 MRB IV, 2215B Garland Avenue, Nashville, Tennessee 37232, Tel: (615) 936-6412; Fax: (615) 936-6410, david.j.calkins@vanderbilt.edu.
[1]**Present Address:**
Department of Pharmaceutical Sciences, Northeast Ohio Medical University, Rootstown, OH 44272, USA.
[2]St. Jude Children's Research Hospital, 262 Danny Thomas Place, Memphis, TN 38105, USA.
[3]University of Arizona, Graduate Program in Neuroscience, 1548 E. Drachman St., P.O. Box 210476, Tucson, AZ 85721, USA.
[4]Department of Psychology and Vanderbilt Vision Research Center, Vanderbilt University, Nashville, TN 37203, USA.

DISCLOSURE STATEMENT
The authors have no conflicts of interest to disclose.

Keywords

neurodegeneration; axonal transport; glaucoma; astrocytes; superior colliculus; brain-derived neurotrophic factor

1.1 INTRODUCTION

Most neurodegenerative disorders involve early signs of axonal dysfunction, including diminished active transport to and from major projection targets in the brain (Adalbert et al., 2009, Morfini et al., 2009). The same is so of the optic neuropathies, the most common of which is glaucoma. Glaucoma is the leading cause of irreversible blindness worldwide and is characterized by progressive degeneration of the retinal ganglion cell (RGC) projection to the brain (Nickells, 1996, Quigley, 1999, Quigley and Broman, 2006, Kwon et al., 2009, Susanna, 2009, Crish and Calkins, 2011). Age and sensitivity to intraocular pressure (IOP) are important risk factors for the disease (Gordon et al., 2002), so animal models that incorporate these are most useful.

The DBA/2J inbred mouse model of hereditary glaucoma presents age-dependent variations in IOP due to mutations that affect fluid flow in the anterior eye (Danias et al., 2003, Schuettauf et al., 2004, Jakobs et al., 2005, Zhou et al., 2005, Inman et al., 2006, Howell et al., 2007). Failure of axonal transport is among the earliest events in the DBA/2J, preceding both degeneration in the optic nerve and RGC somatic loss in the retina (Buckingham et al., 2008, Chidlow et al., 2011, Calkins, 2012). Deficits in anterograde transport from the retina appear earliest at the most distal RGC projection site in the superior colliculus (SC) and progress to more anterior sites over time (Crish et al., 2010). The SC is the primary target for RGC axons in the rodent brain (Hofbauer and Drager, 1985), and a robust complement of RGC axon terminals and their post-synaptic neurons persist there long after transport is completely depleted, which we have described quantitatively (Crish et al., 2010).

Both in the DBA/2J and an inducible model, deficits in anterograde transport progress from one retinotopic sector of the SC to the next (Crish et al., 2010), much like the progression of vision loss in human glaucoma (Goldblum and Mittag, 2002). Age is the predominant determinant of transport depletion, with elevated IOP as an additional stressor that biases the system towards dysfunction (Crish et al., 2010). The sectorial pattern of transport loss in the SC is similar to markers for RGC somatic and axonal pathology in animal models and to topographical loss of RGCs in human glaucomatous retinas (Jakobs et al., 2005, Schlamp et al., 2006, Reichstein et al., 2007, Lei et al., 2009).

Interestingly, we found that even well after axonal transport to the SC is completely depleted, key synaptic structures in the RGC projection persist (Crish et al., 2010). Neural targets in the brain respond to degenerative stressors like diminished transport with mechanisms thought to aid in retention and/or recovery of afferent input that may include remodeling to compensate for loss (Kimura et al., 2006, Endo et al., 2007, Hennigan et al., 2007, Song et al., 2008). For example, after NMDA-induced excitotoxic RGC loss, both brain-derived neurotrophic factor (BDNF) and the astrocytic marker glial fibrillary acidic protein (GFAP) increase within the retinal recipient zone of the SC (Tanaka et al., 2009). Increases in target site BDNF may occur prior to overt degeneration in Alzheimer's disease (Kimura et al., 2004), leading us to question if a similar mechanism is at play within the SC in response to transport failure induced by glaucomatous injury.

1.2 EXPERIMENTAL PROCEDURES

1.2.1 Animals

DBA/2J and its transgenic control strain D2-*Gpnmb*$^{+}$ (Howell et al., 2007) were obtained along with C57BL/6 mice from Jackson Laboratories (Bar Harbor, ME). All experimental procedures were approved by The Vanderbilt University Medical Center Institutional Animal Care and Use Committee. Animals were maintained in a 12h light-dark cycle with standard rodent chow available *ad libitum*. We measured IOP in a subset of DBA/2 mice up to 10 months of age using the Tono-Pen XL (Medtronic Solan) as described previously (Inman et al., 2006).

1.2.2 Microbead occlusion model

To induce elevation of IOP in the rat eye, we utilized microbead occlusion as described (Sappington et al., 2010). Baseline IOP measurements were obtained in awake behaving rats for at least 2 consecutive days prior to microbead surgery using Tono-Pen XL (Medtronic Solan). Experimental IOP readings began 24 hours post-microbead surgery and continued daily until termination of the experiment. To inject microbeads, animals were anesthetized with 2.5% isoflurane (Minrad Inc.) and pupils dilated with 1% tropicamide ophthalmic solution, (Bausch and Lomb). Anesthetic drops (0.5% proparacaine hydrochloride, Bausch and Lomb) were applied to each eye. Using a pulled glass micropipette (tip diameter 100μm; World Precision Instruments), we injected 5 μl of sterile saline (Fisher Scientific) in the anterior chamber of the control eye and 5 μl of 15 μm polystyrene microbeads (Molecular Probes) in the anterior chamber of the experimental eye. We placed antibiotic drops (0.5% moxifloxacin hydrochloride ophthalmic solution; Alcon) on each eye, and the animal recovered for 24 hours prior to resumption of IOP measurements.

1.2.3 Anterograde Transport

Animals were anesthetized with 2.5% isoflurane using a table top anesthesia system (VetEquip, Inc., Pleasanton, CA). Mice received an intravitreal injection of 1 μl of a 1% solution of Cholera toxin subunit β (CTB) conjugated to Alexa Fluor 594 (Invitrogen, Carlsbad CA) or Alexa Fluor 488 (Invitrogen). Forty-eight hours later animals were deeply anesthetized with an overdose of Nembutal (200 mg/kg, Henry Schein, Inc., Indianapolis, IN) and perfused intracardially with phosphate buffered saline (PBS) followed by 4% paraformaldehyde in PBS. Brains were removed and cryoprotected in 30% sucrose overnight and 50 μm coronal slices were taken on a freezing sliding microtome. CTB signal in serial SC sections was digitally photographed on an Olympus AX-70 microscope and intensity of label quantified using ImagePro (Media Cybernetics, Bethesda, MD), as previously described (Crish et al., 2010). Label density from every other section was combined into a colorimetric representation of CTB signal across the collicular retinotopic map (Lambert et al., 2011).

1.2.4 Immuno-chemistry

Immuno-labelling of brain sections was performed as described previously ((Sappington et al., 2009, Crish et al., 2010). We used an antibody against BDNF that strongly recognizes the internal domain of the mature form of the protein and with lesser affinity the immature form (BDNF N-20, 1:200, sc-546, Santa Cruz Biotechnology, Santa Cruz, CA; (Tongiorgi et al., 2004)). Immature BDNF was detected using an antibody specific for pro-BDNF (1:100, sc-65513, Santa Cruz Biotechnology). Antibodies against estrogen-related receptor β (ERRβ, 1:500, E0156, Sigma-Aldrich, St. Louis, MO) and vesicular glutamate transporter 2 (VGluT2, 1:500, 135403, Synaptic Systems, Gottingen, Germany) were used to visualize the RGC axonal projection and axon terminals as described (Crish et al., 2010). Monoclonal

antibodies against GFAP (1:500, MAB360, Millipore, Temecula, CA) and phosphorylated heavy chain neurofilament (SMI-31, 1:1000, SMI-31R, Covance, Emeryville, CA) was used to identify astrocytes and SC neurons and processes (Wilms and Bahr, 1995), respectively. Wide-field fluorescent images were taken on an Olympus AX-70 microscope. Confocal images were taken using a Zeiss LSM510 Meta upright confocal microscope. Photomicrographs were analyzed using a custom-written macro in ImagePro (Media Cybernetics) that determined the percent area of positive label.

1.2.5 Transmission Electron Microscopy

Animals were perfused as described above with the addition of 2% glutaraldehyde to the fixative. Brains were removed and 125 μm^3 samples containing the SC were dissected and embedded in Epon resin as described previously (Yao et al., 2002, Calkins et al., 2005). Ultrathin sections were taken and imaged on a Philips EM-12 Transmission Electron Microscope.

1.2.6 Differential Transport in SC: Micro-dissection and Quantitative PCR (qPCR)

Intravitreal CTB injections were performed in 8 DBA/2J mice between the ages of 5 to 11 months as described above. After 48 hours, animals were euthanized by cervical dislocation, the brain was removed, and cortex overlying the SC was dissected away to expose the midbrain. The SC layers containing RGC projections and their terminals were separated from the deeper SC and immersed in RNAlater (Ambion, Austin, TX). Within three minutes, each superficial SC was flat-mounted on a slide, viewed under an Olympus AX-70 microscope and micro-dissected into areas with (intact) and without (depleted) CTB label. From these animals, we identified 10 individual SC suitable for RNA extraction.

The two micro-dissected samples (intact and depleted CTB) from each SC were RNA-extracted as previously described (Hanna and Calkins, 2006). Briefly, after overnight incubation in lysis buffer (10mM Tris/HCl, pH 8.0; 0.1mM EDTA, pH8.0; 2% SDS, pH 7.3; and 500 μg/ml Proteinase K (Clontech Labs, Mountain View, CA)), RNA was extracted using Trizol reagent (Invitrogen) with 10 μg of glycogen added as an RNA carrier prior to precipitation. RNA concentration and purity were determined using a NanoDrop 8000 spectrophotometer (Thermo Scientific, Wilmington, DE). Samples (1 μg) were DNase-treated (Invitrogen) prior to cDNA synthesis (Applied Biosystems reagents, Foster City, CA), and quantitative PCR (qPCR) was performed using an ABI PRISM 7300 Real-Time PCR System and FAM dye-labelled gene-specific probes for *Bdnf, Camk2a, c-fos, Dctn, GFAP, Syn1*, and *Tau* (Applied Biosystems). Cycling conditions and cycle threshold values were automatically determined by the supplied ABI software (SDS v1.2). Relative product quantities for each transcript were performed in triplicate, normalized to 18s rRNA as an endogenous control, and determined using the $2^{\Delta\Delta C_t}$ analysis method (Livak and Schmittgen, 2001). Data are presented as the ratio of gene expression in the region with depleted transport to that in the region with intact transport for each SC. Significance was calculated using a non-parametric ratio test (chi-square).

For whole tissue qPCR, RNA was extracted as described from the retina, myelinated optic nerve, and SC from each of 5 C57BL/6 animals (3 mo). The two retinas, nerves and SC from each animal were pooled as a single sample. *Bdnf* expression was calculated relative to 18s rRNA in triplicate for each sample, as described above.

1.2.7 Fluorescent *in situ* hybridization

To generate *Bdnf* probes, total RNA from C57BL/6 mouse brain was extracted using RNeasy Mini Kit (Qiagen Inc. USA, Valencia, CA) and first-strand cDNA synthesis performed using Superscript III reverse transcriptase (Invitrogen). Antisense probes for *Bdnf*

mRNA were made against a nucleotide sequence present in all splice variants of mouse *Bdnf* (nucleotides 326 to 750 of [GenBank: NM_001048142]). Transcript generated by PCR using primers to BDNF (forward 5'-AGA GCT TTG TGT GGA CCC TGA GTT-3' and reverse 5'-CCC TCA TAG ACA TGT TTG CGG CAT-3') was inserted into pGEM-T Easy Vector (Promega, Madison, WI) and orientation verified by sequencing. Isolated plasmids were linearized and purified, and labelled BDNF RNA probes generated using SP6 and T7 RNA polymerases and Dioxigenin RNA Labelling Mix (Roche Applied Sciences; Indianapolis, IN). Probe concentration and quality (A_{260}/A_{280} ratio) were determined using a NanoDrop spectrophotometer. Probes were stored at −80°C.

Mice were perfused and coronal sections (50 μm) taken as described above (section 1.2.4). Tissue was washed in 0.75% glycine followed by 0.3% triton X-100, and then treated with 1 μg/ml proteinase K (Sigma-Aldrich) at room temperature for 5 minutes. Sections were acetylated in 0.25% acetic anhydride/0.1M triethanolamine (pH 8.0) for 10 minutes and rinsed. Tissue was pre-hybridized for one hour at 58°C in hybridization solution (50% formamide, 5X SSC, 2% blocking reagent (Roche), 0.1% N-lauroylsarcosine (NLS) (Sigma-Aldrich) and 0.1% SDS). Probes (2 ng/μl) were denatured at 80°C for 10 minutes in hybridization solution prior to incubation with brain sections at 58°C overnight. Tissue was then washed and treated with 20 μg/ml RNase A (Macherey-Nagel, Bethlehem, PA) in 10mM Tris (pH 8.0), 1mM EDTA and 0.5M NaCl for 10 minutes at 37°C to remove excess probe. Immmunodetection of labelled BDNF mRNA was performed using anti-DIG-F_{ab}-POD conjugate (Roche) diluted 1:100 in blocking buffer (1% blocking reagent (Roche) in 0.1M Tris (pH 7.5), 0.15M NaCl) followed by detection using the TSA plus Fluorescein system (Perkin-Elmer; Boston, USA). Immmunolabelling was performed with antibodies to GFAP (1:500, Z0334, DAKO, Carpinteria, CA) and phosphorylated heavy chain neurofilament (1:1000, SMI-31) as described above. Confocal images were taken using an Olympus FV-1000 inverted confocal microscope.

1.2.8 Subcellular Fractionation and Western Blotting

We performed subcellular fractionation of homogenate obtained from the superficial region of the DBA/2J SC as described previously with minor modifications (Huttner et al., 1983, Blackstone et al., 1992, Fawcett et al., 1997). The superficial layer of the SC was dissected from fresh DBA/2J brain and immediately immersed into HEPES-buffered sucrose [0.32M sucrose, 4mM HEPES, pH 7.4, 0.1 mM PMSF, 1mM benzamidine-HCl, 2mM EGTA, 1mM sodium vanadate, 50mM sodium fluoride] containing protease and phosphatase inhibitors (Roche Diagnositcs, Indianapolis IN). Tissue was homogenized and then centrifuged for 10 minutes at 1000×g to remove nuclei and large debris and then for 15 minutes at 10,000×g to yield a light plasma membrane pellet consistent with synaptosome isolation. For lysis, this pellet fraction was resuspended in ice cold water containing protease and phosphatase inhibitors, homogenized and then adjusted to 4mM HEPES and pH 7.4 with 0.1M HEPES-NaOH. Following 30 minute incubation on ice, the suspension was centrifuged at 25,000×g for 20 minutes to yield the lysed light-membrane pellet (LP3) and a crude vesicle supernatant fraction, which was then centrifuged at 165,000×g for 2 hours to yield a supernatant of released vesicle content (LS4) and a vesicle-enriched pellet (P4). Samples of fractions LP3, LS4 and P4 containing approximately 40 μg of protein were separated on 15% Tris-HCl Criterion gel (Bio-Rad) by SDS-PAGE using standard SDS sample buffer containing 0.1M dithiothreitol. Proteins were transferred onto PVDF membranes (Immobilon-FL, Millipore) and blots were probed with antibodies against the synaptic vesicle membrane protein synaptotagmin I (1:750, Acris Antibodies), BDNF (N-20) (1:200, Santa Cruz), and β-Actin (1:2000, Ambion).

1.3 Results

1.3.1 Focal Increases in BDNF with Transport Loss

Previously we demonstrated that deficits in anterograde transport to the DBA/2J SC progress in retinotopic sectors and increase in likelihood and severity with age; age-dependent elevation in IOP is an additional stressor but not the primary predictor (Crish et al., 2010). The SC from the C57BL/6 (C57) and D2-*Gpnmb*$^{+}$ non-glaucomatous mouse strains and a 3-month DBA/2J exhibited intact CTB signal across the superficial SC (sSC; Figure 1A). This is reflected in the complete retinotopic representation of CTB signal for these SC (Figure 1A, insets). In contrast, SC from 8, 10 and 12 month DBA/2J mice demonstrated increasingly depleted CTB signal indicating diminished anterograde transport (Figure 1B). For these, transport depletion followed a sectorial progression filling from the peripheral field to the representation of the optic disk gap (Figure 1B), consistent with our published observations (Crish et al., 2010).

Next we tested whether depletion of transport signal was accompanied by changes in levels of BDNF, as has been described for the SC with NMDA-induced RGC loss (Tanaka et al., 2009). In normal C57 SC, BDNF immuno-labelling was strongest in the deep layers of the SC, with only sporadic signal in the superficial layers where RGC axons terminate and no detectable co-localization with transported CTB (Figure 2A). In a 3 mo DBA/2J, BDNF label remained uniform in the deep SC, like the C57, but increased in the RGC-recipient zone coincident with a focal transport deficit near the midline (Figure 2B). Across ages of DBA/2J, BDNF localization increased focally wherever CTB signal in the superficial SC was depleted (Figure 2C, D). Even as BDNF levels rose in the RGC-recipient zone, levels in the deeper layers remained the same (Figure 2D). In removing the cortex during dissection, often we retained a sharp delineation of the dorsal border of superficial layer 1 of the SC, which is primarily astrocytic (Harvey et al., 1993). This border was generally marked by strong BDNF localization (Figures 2B,C).

The coincident increase in BDNF with transport loss was not confined to the DBA/2J. Previously we demonstrated that deficits in anterograde transport to the SC similar to those in the DBA/2J could be induced by elevating IOP in the rat eye by injection of inert microspheres into the anterior chamber (Crish et al., 2010). Here, over a 5 week period microbead injection elicited a 35% elevation in IOP compared to IOP in the opposing eye, which received an equivalent-volume injection of saline (Figure 3A; $p<0.001$). This elevation induced a focal deficit in CTB transport (Figure 3B, left panel), similar to the sectorial depletion we previously described in this model (Crish et al., 2010). As in the DBA/2J, loss of transport was accompanied by increased BDNF in the superficial SC, spatially coincident with the region of diminished CTB signal (Figure 3B, right panels). For areas with intact transport, most BDNF was contained in the deeper SC, as in the DBA/2J (Figure 2).

1.3.2 Hypertrophy of BDNF-Containing Astrocytes

In the DBA/2J SC, BDNF levels remained modest in the RGC-recipient zone if CTB signal was intact, even if elsewhere in the SC transport was depleted (Figure 4A). Thus, changes in BDNF were mostly restricted in terms of spatial distribution. With loss of CTB signal, the increase in BDNF appeared at least in part to originate in astrocyte processes, especially those encroaching the RGC-recipient zone from the dorsal ridge (Figure 4B). For a 10 mo DBA/2J, complete depletion of CTB signal was accompanied by hypertrophy of BDNF-expressing astrocytes labelled by GFAP along the midline separating the SC for the left and right optic projections (Figure 4C). This same transport-depleted SC demonstrated even more profound hypertrophy of astrocytes labelled for BDNF along the dorsal ridge

containing layer 1 (Figure 4D). Even with increased astrocyte BDNF, it was most abundant in the underlying neuropil of the SC. Compared to C57, even regions of the DBA/2J SC with intact CTB signal demonstrated both increased BDNF (67%) and GFAP (51%), though neither difference was significant (Figure 4E; p=0.061 and 0.187, respectively). In regions of the DBA/2J SC with depleted transport, BDNF increased 120% and GFAP 239% compared to the C57 (p<0.001) and by 32% (BDNF, p=0.027) and 124% (GFAP, p<0.001) compared to regions of the same SC with intact CTB transport (Figure 4E).

Confocal images of a single thin plane through the 10 mo DBA/2J SC shown in Figure 4C suggests that astrocyte BDNF was largely cytoplasmic in origin and distributed nearly uniformly throughout the astrocyte (Figure 5A). In a higher magnification single plane through an 8 mo DBA/2J SC, BDNF appeared to distribute in pockets of focal concentration within the astrocyte (Figure 5B). In orthogonal views of this plane, BDNF clearly was internalized and not generally associated with the astrocyte membrane. Finer astrocyte processes including end-feet near SC neuronal processes did not appear to contain appreciable amounts of BDNF (Figure 5B, side images).

In SC with intact CTB transport, GFAP-labelled astrocytes were most prominent along the dorsal ridge of superficial layer 1 (Figure 6A). The retinal recipient zone of the superficial SC itself contained relatively low levels of GFAP, as did the deep SC, which contains a visual map but lacks a direct retinal projection. GFAP label along the midline between the two SC distributed evenly, reflecting the symmetry in intact CTB signal (Figure 6A, right panel). An 8-month DBA/2J with intact transport in one SC and near complete depletion in the other demonstrated a unilateral increase in GFAP label and astrocyte hypertrophy in both the superficial and deep SC (Figure 6B). These changes were coincident with transport loss, but prior to overt degeneration. A 10 mo SC with no remaining CTB signal and considerable astrocyte hypertrophy in the superficial recipient zone retained an intact distribution of RGC axon terminals visualized either with antibodies against estrogen related receptor beta (ERRβ; Figure 6C) or vesicular glutamate transporter 2 (VGluT2; Figure 6D). Both ERRβ and VGluT2 labelling indicate persistence of RGC axons and their terminals in the DBA/2J SC, which are retained nearly *in toto* up to 22 months, long after complete depletion of anterograde transport at 11–12 months; this is quantified extensively in our previous work (Crish et al., 2010).

This structural persistence is reiterated at the ultrastructural level in electron micrographs (Figure 7). For a 12 month SC organization was completely intact (Figure 7A), and we identified the axon terminals from RGCs (RLP), inhibitory intracollicular terminals (F), and cortico-collicular projections (RSD) based on established morphological criteria (Valverde, 1973, Calkins et al., 2005). The 12 month SC included clear synaptic active zones between RLP terminals and the dendrites of collicular relay neurons (Figure 7A). For a 15 month SC, RLP terminals remained intact and formed pre-synaptic active zones, but appeared slightly dystrophic (Figure 7B). This is consistent with our earlier work in which we quantified persistence of SC synaptic structures for a limited interval after anterograde transport depletion (see Figure 7 in Crish et al., 2010).

1.3.3 Changes in Gene Expression with Loss of Anterograde Transport

We used quantitative PCR to measure changes in gene expression associated with loss of anterograde transport. Under fluorescent illumination, we micro-dissected RGC-recipient regions with depleted CTB signal vs. regions with intact CTB (Figure 8A, B). In completely intact SC, expression of *Bdnf* mRNA is several-fold higher than in optic nerve and retina (Figure 8C). Surprisingly, in the DBA/2J SC the ratio of *Bdnf* mRNA for depleted vs. intact transport was actually below unity, indicating a significant decrease in expression with transport loss (mean ratio of 0.658; p=0.008). Similarly, depleted transport was associated

with significantly diminished expression of dynactin (*Dctn*; ratio of 0.784, p=0.0004), a microtubule and dynein-binding protein involved in axonal transport. Expression of *Tau* also decreased with transport loss (0.746, p=0.017), suggesting changes in microtubule stabilization. The only genes with mean expression ratios greater than unity were *Gfap* (1.459) and *c-fos* (1.185), a marker for neural activity. However, both were highly variable between colliculi (p=0.206 and 0.289, respectively).

As expected based on persistence of RGC axon terminals (section 1.3.2, Figure 6 C,D), the ratio for genes associated with synaptic structures did not change with transport loss and was close to unity. This was true for both the presynaptic protein synapsin (*Syn1*; ratio of 0.924) and its phosphorylating agent calcium/calmodulin-dependent protein kinase type II alpha (*Camk2a*; ratio of 0.838). Levels of these genes were statistically similar between regions with and without transport (p>0.16).

To confirm our RT-PCR results, we performed fluorescent *in situ* hybridization for *Bdnf* mRNA in conjunction with cell-specific markers. In C57 colliculus, *Bdnf* localization was clear in neurons labelled for phosphorylated heavy chain neurofilament (pNF, Figure 9A); a control sense sequence elicited no label as expected (Figure 9B). The *Bdnf* transcript also localized within GFAP-expressing astrocyte cell bodies along the dorsal border of superficial layer 1; this was far less prominent in the retinorecipient zone of the superficial SC (Figure 9A,C). A similar pattern was observed in 3-month DBA/2J (Figure 9C). In 9-month DBA/2J mice, *Bdnf* signal appeared greatly diminished compared to both the C57 and 3-month DBA/2J (Figure 9D), consistent with the PCR results (Figure 8). Single plane images through the RGC-recipient layer revealed *Bdnf* localized to pNF^+ neurons enveloped heavily by astrocyte processes (Figure 9E).

The apparent contradiction between increased BDNF protein and diminished *Bdnf* mRNA could be explained if the BDNF label actually represents detection of its immature form (pro-BDNF). However, in C57 SC, antibodies specific for pro-BDNF elicit very little co-localized signal with GFAP-labelled astrocytes (Figure 10A). Furthermore, in the RGC recipient zone, most pro-BDNF was contained within small, irregular shaped cells that resemble microglia. The exception was the dorsal border of the SC and the midline between the two colliculi, where a thin but intense band of co-localization with GFAP was observed. In both 8 mo and 10 mo DBA/2J SC (Figures 9B–C), pro-BDNF did not localize in hypertrophic astrocytes but was most apparent in small cells whose morphologies we could not discern. Like the C57, co-localization was modest and restricted to the SC border and midline.

Finally, we performed western blots of subcellular fractions of the superficial layer of the DBA/2J SC to determine possible sources of BDNF, using detection of β-actin as a positive control (Figure 11). As expected, detection of the synaptic vesicle protein synaptotagmin was most prominent in the synaptosomal membrane fraction (Figure 11, left panel), but absent in the supernatant of released vesicle content (Figure 11, right panel). Interestingly, compared to younger DBA/2J SC, synaptotagmin was significantly diminished in the vesicle membrane fraction of 10 mo tissue (Figure 11, middle panel), which could indicate depletion of available pools during progression. In contrast, detection of BDNF was very low and decreased with age in the synaptosomal fraction and completely absent in the vesicle membrane fraction. It was, however, highly concentrated in the released vesicle supernatant (Figure 11, right panel). Taken together, these results suggest that most BDNF in the SC is sequestered within vesicles.

1.4 Discussion

The SC is the primary target for RGC axons in rodents, forming a complete and highly regular retinotopic representation of visual space (Hofbauer and Drager, 1985). Both in the DBA/2J and an inducible model of glaucoma (microbead occlusion), deficits in axonal transport to the SC progress retinotopically, like vision loss in glaucoma, and precede outright degeneration of the retinal projection (Buckingham et al., 2008; Crish et al., 2010). Age is the primary stressor associated with transport loss, with elevated IOP serving as an additional bias towards dysfunction (Figure 1; Crish et al., 2010).

Our current experiments demonstrate that BDNF increases focally in the retinorecipient region of the SC, coincident with areas of depleted transport of CTB (section 1.3.1, Figures 2 and 3). BDNF signal increased both in neuronal processes and along with increased GFAP in hypertrophic astrocytes (section 1.3.2, Figure 4). Thus, both GFAP and BDNF elevations could be triggered in concert either by transport dysfunction or an associated event. BDNF in astrocytes appeared to be internalized, largely within pockets reminiscent of endosomes (Figure 5). While shrinkage and loss of retinal target neurons in the thalamus occurs later in progression (Yucel and Gupta, 2008), we show that astrocyte hypertrophy coincides with transport depletion and precedes loss of synaptic structures or changes in expression of synapse-related genes (sections 1.3.2 and 1.3.3, Figures 6–8), paralleling other neurodegenerative diseases (Adalbert et al., 2009, Morfini et al., 2009). Coincident increases in BDNF and astrocyte hypertrophy might represent an intrinsic mechanism to ameliorate the progression of pathology or mitigate the effects of axon damage, as described in other systems (Kimura et al., 2006, Endo et al., 2007, Hennigan et al., 2007, Song et al., 2008). NMDA-induced excitotoxicity in the retina also increases BDNF and GFAP in retinal brain targets (Tanaka et al., 2009); similar neurochemical changes in retinal targets occur in animal models utilizing acute elevations in ocular pressure (Sasaoka et al., 2008, Zhang et al., 2009). Thus, our finding suggests a more global mechanism for how retinorecipient targets respond to disease-relevant stressors.

The structural persistence following axonal dysfunction has profound implications for developing therapies. Restoring function to intact neuronal pathways is a much more tractable and attractive target for intervention than replacing neurons or long stretches of axons. We also observed a modest level of astrocyte hypertrophy with transport loss in the non-retinorecipient SC (section 1.3.2, Figure 6), which could be due to dysfunctional signalling from extra-retinal sources of visual input. As the retinotopic map is coarser in the deep SC, one would expect less topographical constraint in dysfunction-induced responses. Expression of genes encoding synaptic structures in the SC remained unchanged with transport loss (section 1.3.3, Figure 8), consistent with a period of structural persistence (Figure 6, (Crish et al., 2010)). However, expression of *Bdnf* mRNA diminished, as detected by both PCR (Figure 8) and in situ hybridization (section 1.3.3, Figure 9). This decrease occurred in contrast to the obvious increase in BDNF protein with transport loss (sections 1.3.1 and 1.3.2, Figures 2–4). Disparities between levels of BDNF protein and mRNA have been reported in other models of neurodegeneration (Nawa et al., 1995, Lee et al., 2002), which may indicate a common neuronal response to injury.

Interestingly, the *Bdnf* anti-sense probe was detected most strongly within collicular neurons rather than astrocytes in the RGC recipient zone (section 1.3.3, Figures 8), despite the latter's high levels of BDNF protein. We designed our *Bdnf* anti-sense to recognize a nucleotide sequence common to all known splice variants of mouse *Bdnf* (see section 1.2.7). Thus, our finding would seem to suggest that increased BDNF immuno-labelling in astrocytes was not due to *de novo* synthesis. It is possible that BDNF is undergoing increased translation in the SC despite limited gene expression or that the protein itself is

being sequestered following limited translation thereby resulting in accumulation within astrocytes and collicular neurons. New experiments are necessary to test these ideas. Another possibility suggested by a recent study of mouse hippocampus is the uptake by astrocytes of extracellular BDNF released from collicular neurons (Matsumoto et al., 2008). This seems plausible, since BDNF increased in the neuropil of the RGC recipient zone with transport loss (sections 1.3.1 and 1.3.2, Figures 2–4). Astrocytes could then sequester external BDNF in response to diminished transcription in collicular neurons, possibly for re-release to strengthen synaptic structures (Lessmann et al., 2003, Bergami et al., 2008).

Another possibility suggested by the literature is that collicular neurons release pro-BDNF, which astrocytes would sequester, process and re-release as mature BDNF (Bergami et al., 2008, Yang et al., 2009). However, labelling with antibodies that specifically recognize pro-BDNF showed only modest signal in collicular neurons (section 1.3.3, Figure 10). This is meaningful especially when compared to the large number of SC neurons expressing *Bdnf* mRNA, as revealed by in situ hybridization (section 1.3.3, Figure 9). Moreover, GFAP-labelled astrocytes in the RGC recipient zone did not contain pro-BDNF (section 1.3.3, Figure 10). Taken together, these results suggest that the BDNF signal we detected in astrocytes is not attributable to cross-reactivity with pro-BDNF. This is in agreement with careful control studies of the BDNF antibody we used that showed very low affinity for pro-BDNF (Tongiorgi et al., 2004).

Though BDNF was contained in the RGC recipient zone of the SC, we observed little if any co-localization of BDNF protein within CTB-containing RGC axon terminals (sections 1.3.1 and 1.3.2, Figures 2 and 4). Results from the subcellular fractionation experiment indicate that synaptosomal membrane BDNF is relatively low in concentration and decreases in the SC with age (section 1.3.3, Figure 11). However, BDNF released from vesicles represents the highest fraction and does not change. In other brain regions, BDNF can be stored in and released from secretory dense-core vesicles (Dieni et al., 2012), with highly spatially-specific exocytosis from both axonal and dendritic compartments in response to perturbations in neuronal activity (Dean et al., 2012). Thus, perhaps vesicle-stored BDNF in SC neurons is released in response to diminished RGC axonal transport and subsequent stress to synaptic activity.

Disruptions in neurotrophin signaling, including BDNF, have been extensively implicated in a variety of neurodegenerative diseases and traumatic injury (Oyesiku et al., 1999, Dougherty et al., 2000, Song et al., 2008, Zuccato and Cattaneo, 2009). It is presumed that intrinsically protective mechanisms must at some level utilize the actions of trophic factors, which now represent actively pursued therapeutic avenues (Zuccato and Cattaneo, 2009). Nevertheless, application or upregulation of BDNF has had limited success in animal models of Alzheimer’s, Parkinson’s, and Huntington’s diseases (Ando et al., 2002, Zuccato and Cattaneo, 2007), in spinal cord injury (McTigue et al., 1998), and in experimental autoimmune encephamyelitis (De Santi et al., 2009). Similar to the results we report, a recent study demonstrated that over-expression of astrocyte-driven BDNF conserved striatal synaptic structures in a mouse model of Huntington’s disease (Giralt et al., 2011).

In the visual system, exogenous BDNF application to the eye exhibits only limited and temporary protection after optic nerve crush or transection (Di Polo et al., 1998, Chen and Weber, 2004, Parrilla-Reverter et al., 2009). Combined BDNF application to both the eye and brain is more effective in protecting RGCs, suggesting that targeting the brain may have potential therapeutic uses in eye disease (Weber et al., 2010). In glaucoma, disrupted BDNF transport from the brain to the eye has been implicated in pathogenesis (Pease et al., 2000, Quigley et al., 2000), which is likely to include early degradation of axonal cytoskeleton at the optic nerve head (Chidlow et al., 2011). However, much like acute optic nerve injury,

BDNF application to the glaucomatous eye has demonstrated limited capacity for neuroprotection (Ko et al., 2000, Ko et al., 2001). Given BDNF's role in synaptic survival and neurite maintenance (Lessmann et al., 2003, Song et al., 2008), a better approach to realizing its therapeutic potential might be to link BDNF more directly to intrinsic mechanisms that contribute to persistence of RGC axonal structures following loss of active transport.

The current study did not address how deficits in axonal transport in the SC might modulate expression of the high-affinity tyrosine receptor kinase TrkB. Activation of TrkB by BDNF affects several intracellular cascades that influence neuronal repair and survival, and so modulation of the receptor is of interest from a therapeutic standpoint (Fenner, 2012). The truncated isoform of TrkB, TrkB.t1, is also widely distributed throughout the brain and is expressed not only in neurons, but in different populations of astrocytes (Ohira et al., 2005). Most importantly, from the standpoint of this study, TrkB.t1 is thought to sequester and internalize BDNF for later release. In hippocampal astrocytes, TrkB.t1 at the plasma membrane was shown to bind BDNF from the extracellular domain and mediate its endocytosis prior to release into the extracellular space (Alderson et al., 2000). This pathway could ostensibly contribute to focal sequestration and re-release of BDNF from astrocytes in response to depleted axonal transport in the SC. Further experimentation is needed to determine whether such a mechanism is relevant in the models we explored.

1.5 Conclusions

Secondary degeneration of target sites in the brain is generally thought to be either concurrent with or just subsequent to loss of primary input. We have shown using models of glaucoma that focal deficits in anterograde axonal transport from the retina to the superior colliculus induce a concurrent elevation of BDNF, especially in hypertrophic astrocytes, that is spatially coincident with the retinotopic location of transport loss. This elevation may reflect a local intrinsic pathway to slow loss of retino-collicular synapses, which are retained well after axonal transport is completely depleted by disease-relevant stressors.

Acknowledgments

We thank Mrs. Ann Gearon and Mr. Brian J. Carlson for their assistance with intraocular pressure measurements.

ROLE OF THE FUNDING SOURCE

The Supported by NIH EY017427 (DJC), the Melza M. and Frank Theodore Barr Foundation through the Glaucoma Research Foundation (DJC), a Departmental Unrestricted Award from Research to Prevent Blindness, Inc. (DJC), an American Health Assistance Foundation National Glaucoma Research Award (DJC), Fight for Sight (SDC), the Vanderbilt Discovery Science program (DJC), and Vanderbilt Vision Research Center (P30EY008126).

ABBREVIATIONS

SC	superior colliculus
BDNF	brain-derived neurotrophic factor
RGC	retinal ganglion cell
IOP	intraocular pressure
GFAP	glial fibrillary acidic protein
CTB	cholera toxin subunit β
ERRβ	estrogen-related receptor β

VGluT2	vesicular glutamate transporter 2
Dctn	dynactin
Syn1	synapsin
Camk2α	calcium/calmodulin-dependent protein kinase type II alpha

REFERENCES

Adalbert R, Nogradi A, Babetto E, Janeckova L, Walker SA, Kerschensteiner M, Misgeld T, Coleman MP. Severely dystrophic axons at amyloid plaques remain continuous and connected to viable cell bodies. Brain. 2009; 132:402–416. [PubMed: 19059977]

Alderson RF, Curtis R, Alterman AL, Lindsay RM, DiStefano PS. Truncated TrkB mediates the endocytosis and release of BDNF and neurotrophin-4/5 by rat astrocytes and schwann cells in vitro. Brain Res. 2000; 871(2):210–222. [PubMed: 10899288]

Ando S, Kobayashi S, Waki H, Kon K, Fukui F, Tadenuma T, Iwamoto M, Takeda Y, Izumiyama N, Watanabe K, Nakamura H. Animal model of dementia induced by entorhinal synaptic damage and partial restoration of cognitive deficits by BDNF and carnitine. J Neurosci Res. 2002; 70:519–527. [PubMed: 12391613]

Bergami M, Santi S, Formaggio E, Cagnoli C, Verderio C, Blum R, Berninger B, Matteoli M, Canossa M. Uptake and recycling of pro-BDNF for transmitter-induced secretion by cortical astrocytes. J Cell Biol. 2008; 183:213–221. [PubMed: 18852301]

Blackstone CD, Moss SJ, Martin LJ, Levey AI, Price DL, Huganir RL. Biochemical characterization and localization of a non-N-methyl-D-aspartate glutamate receptor in rat brain. J Neurochem. 1992; 58:1118–1126. [PubMed: 1371146]

Buckingham BP, Inman DM, Lambert W, Oglesby E, Calkins DJ, Steele MR, Vetter ML, Marsh-Armstrong N, Horner PJ. Progressive ganglion cell degeneration precedes neuronal loss in a mouse model of glaucoma. J Neurosci. 2008; 28:2735–2744. [PubMed: 18337403]

Calkins DJ. Critical pathogenic events underlying progression of neurodegeneration in glaucoma. Prog. Retinal and Eye Research. epub Aug 1).

Calkins DJ, Sappington RM, Hendry SH. Morphological identification of ganglion cells expressing the alpha subunit of type II calmodulin-dependent protein kinase in the macaque retina. J Comp Neurol. 2005; 481:194–209. [PubMed: 15562509]

Chen H, Weber AJ. Brain-derived neurotrophic factor reduces TrkB protein and mRNA in the normal retina and following optic nerve crush in adult rats. Brain Res. 2004; 1011:99–106. [PubMed: 15140649]

Chidlow G, Ebneter A, Wood JP, Casson RJ. The optic nerve head is the site of axonal transport disruption, axonal cytoskeleton damage and putative axonal regeneration failure in a rat model of glaucoma. Acta Neuropathol. 2011; 121:737–751. [PubMed: 21311901]

Crish SD, Calkins DJ. Neurodegeneration in glaucoma: progression and calcium-dependent intracellular mechanisms. Neuroscience. 2011; 176:1–11. [PubMed: 21187126]

Crish SD, Sappington RM, Inman DM, Horner PJ, Calkins DJ. Distal axonopathy with structural persistence in glaucomatous neurodegeneration. Proc Natl Acad Sci U S A. 2010; 107:5196–5201. [PubMed: 20194762]

Danias J, Lee KC, Zamora MF, Chen B, Shen F, Filippopoulos T, Su Y, Goldblum D, Podos SM, Mittag T. Quantitative analysis of retinal ganglion cell (RGC) loss in aging DBA/2NNia glaucomatous mice: comparison with RGC loss in aging C57/BL6 mice. Invest Ophthalmol Vis Sci. 2003; 44:5151–5162. [PubMed: 14638711]

De Santi L, Annunziata P, Sessa E, Bramanti P. Brain-derived neurotrophic factor and TrkB receptor in experimental autoimmune encephalomyelitis and multiple sclerosis. J Neurol Sci. 2009; 287:17–26. [PubMed: 19758606]

Dean C, Liu H, Staudt T, Stahlberg MA, Vingill S, Buckers J, Kamin D, Engelhardt J, Jackson MB, Hell SW, Chapman ER. Distinct subsets of Syt-IV/BDNF vesicles are sorted to axons versus

dendrites and recruited to synapses by activity. J Neurosci. 2012; 32:5398–5413. [PubMed: 22514304]

Di Polo A, Aigner LJ, Dunn RJ, Bray GM, Aguayo AJ. Prolonged delivery of brain-derived neurotrophic factor by adenovirus-infected Muller cells temporarily rescues injured retinal ganglion cells. Proc Natl Acad Sci U S A. 1998; 95:3978–3983. [PubMed: 9520478]

Dieni S, Matsumoto T, Dekkers M, Rauskolb S, Ionescu MS, Deogracias R, Gundelfinger ED, Kojima M, Nestel S, Frotscher M, Barde YA. BDNF and its pro-peptide are stored in presynaptic dense core vesicles in brain neurons. J Cell Biol. 2012; 196:775–788. [PubMed: 22412021]

Dougherty KD, Dreyfus CF, Black IB. Brain-derived neurotrophic factor in astrocytes, oligodendrocytes, and microglia/macrophages after spinal cord injury. Neurobiol Dis. 2000; 7:574–585. [PubMed: 11114257]

Endo T, Spenger C, Tominaga T, Brene S, Olson L. Cortical sensory map rearrangement after spinal cord injury: fMRI responses linked to Nogo signalling. Brain. 2007; 130:2951–2961. [PubMed: 17913768]

Fawcett JP, Aloyz R, McLean JH, Pareek S, Miller FD, McPherson PS, Murphy RA. Detection of brain-derived neurotrophic factor in a vesicular fraction of brain synaptosomes. J Biol Chem. 1997; 272:8837–8840. [PubMed: 9082996]

Fenner BM. Truncated TrkB: beyond a dominant negative receptor. Cytokine Growth Factor Rev. 2012; 23(1–2):15–24. [PubMed: 22341689]

Giralt A, Carreton O, Lao-Peregrin C, Martin ED, Alberch J. Conditional BDNF release under pathological conditions improves Huntington's disease pathology by delaying neuronal dysfunction. Mol Neurodegener. 2011; 6:71. [PubMed: 21985529]

Goldblum D, Mittag T. Prospects for relevant glaucoma models with retinal ganglion cell damage in the rodent eye. Vision Res. 2002; 42:471–478. [PubMed: 11853763]

Gordon MO, Beiser JA, Brandt JD, Heuer DK, Higginbotham EJ, Johnson CA, Keltner JL, Miller JP, Parrish RK 2nd, Wilson MR, Kass MA. The Ocular Hypertension Treatment Study: baseline factors that predict the onset of primary open-angle glaucoma. Arch Ophthalmol. 2002; 120:714–720. discussion 829-730. [PubMed: 12049575]

Hanna MC, Calkins DJ. Expression and sequences of genes encoding glutamate receptors and transporters in primate retina determined using 3'-end amplification polymerase chain reaction. Mol Vis. 2006; 12:961–976. [PubMed: 16943768]

Harvey AR, Plant GW, Kent AP. The distribution of astrocytes, oligodendroglia and myelin in normal and transplanted rat superior colliculus: an immunohistochemical study. J Neural Transplant Plast. 1993; 4:1–14. [PubMed: 7509197]

Hennigan A, O'Callaghan RM, Kelly AM. Neurotrophins and their receptors: roles in plasticity, neurodegeneration and neuroprotection. Biochem Soc Trans. 2007; 35:424–427. [PubMed: 17371291]

Hofbauer A, Drager UC. Depth segregation of retinal ganglion cells projecting to mouse superior colliculus. J Comp Neurol. 1985; 234:465–474. [PubMed: 3988995]

Howell GR, Libby RT, Marchant JK, Wilson LA, Cosma IM, Smith RS, Anderson MG, John SW. Absence of glaucoma in DBA/2J mice homozygous for wild-type versions of Gpnmb and Tyrp1. BMC Genet. 2007; 8:45. [PubMed: 17608931]

Huttner WB, Schiebler W, Greengard P, De Camilli P. Synapsin I (protein I), a nerve terminal-specific phosphoprotein. III. Its association with synaptic vesicles studied in a highly purified synaptic vesicle preparation. J Cell Biol. 1983; 96:1374–1388. [PubMed: 6404912]

Inman DM, Sappington RM, Horner PJ, Calkins DJ. Quantitative correlation of optic nerve pathology with ocular pressure and corneal thickness in the DBA/2 mouse model of glaucoma. Invest Ophthalmol Vis Sci. 2006; 47:986–996. [PubMed: 16505033]

Jakobs TC, Libby RT, Ben Y, John SW, Masland RH. Retinal ganglion cell degeneration is topological but not cell type specific in DBA/2J mice. J Cell Biol. 2005; 171:313–325. [PubMed: 16247030]

Kimura N, Negishi T, Ishii Y, Kyuwa S, Yoshikawa Y. Astroglial responses against Abeta initially occur in cerebral primary cortical cultures: species differences between rat and cynomolgus monkey. Neurosci Res. 2004; 49:339–346. [PubMed: 15196782]

Kimura N, Takahashi M, Tashiro T, Terao K. Amyloid beta up-regulates brain-derived neurotrophic factor production from astrocytes: rescue from amyloid beta-related neuritic degeneration. J Neurosci Res. 2006; 84:782–789. [PubMed: 16862545]

Ko ML, Hu DN, Ritch R, Sharma SC. The combined effect of brain-derived neurotrophic factor and a free radical scavenger in experimental glaucoma. Invest Ophthalmol Vis Sci. 2000; 41:2967–2971. [PubMed: 10967052]

Ko ML, Hu DN, Ritch R, Sharma SC, Chen CF. Patterns of retinal ganglion cell survival after brain-derived neurotrophic factor administration in hypertensive eyes of rats. Neurosci Lett. 2001; 305:139–142. [PubMed: 11376903]

Kwon YH, Fingert JH, Kuehn MH, Alward WL. Primary open-angle glaucoma. N Engl J Med. 2009; 360:1113–1124. [PubMed: 19279343]

Lambert WS, Ruiz L, Crish SD, Wheeler LA, Calkins DJ. Brimonidine prevents axonal and somatic degeneration of retinal ganglion cell neurons. Mol Neurodegener. 2011; 6:4. [PubMed: 21232114]

Lee TH, Kato H, Chen ST, Kogure K, Itoyama Y. Expression disparity of brain-derived neurotrophic factor immunoreactivity and mRNA in ischemic hippocampal neurons. Neuroreport. 2002; 13:2271–2275. [PubMed: 12488809]

Lei Y, Garrahan N, Hermann B, Fautsch MP, Johnson DH, Hernandez MR, Boulton M, Morgan JE. Topography of neuron loss in the retinal ganglion cell layer in human glaucoma. Br J Ophthalmol. 2009; 93:1676–1679. [PubMed: 19671529]

Lessmann V, Gottmann K, Malcangio M. Neurotrophin secretion: current facts and future prospects. Prog Neurobiol. 2003; 69:341–374. [PubMed: 12787574]

Livak KJ, Schmittgen TD. Analysis of relative gene expression data using real-time quantitative PCR and the 2(−Delta Delta C(T)) Method. Methods. 2001; 25:402–408. [PubMed: 11846609]

Matsumoto T, Rauskolb S, Polack M, Klose J, Kolbeck R, Korte M, Barde YA. Biosynthesis and processing of endogenous BDNF: CNS neurons store and secrete BDNF, not pro-BDNF. Nat Neurosci. 2008; 11:131–133. [PubMed: 18204444]

McTigue DM, Horner PJ, Stokes BT, Gage FH. Neurotrophin-3 and brain-derived neurotrophic factor induce oligodendrocyte proliferation and myelination of regenerating axons in the contused adult rat spinal cord. J Neurosci. 1998; 18:5354–5365. [PubMed: 9651218]

Morfini GA, Burns M, Binder LI, Kanaan NM, LaPointe N, Bosco DA, Brown RH Jr, Brown H, Tiwari A, Hayward L, Edgar J, Nave KA, Garberrn J, Atagi Y, Song Y, Pigino G, Brady ST. Axonal transport defects in neurodegenerative diseases. J Neurosci. 2009; 29:12776–12786. [PubMed: 19828789]

Nawa H, Carnahan J, Gall C. BDNF protein measured by a novel enzyme immunoassay in normal brain and after seizure: partial disagreement with mRNA levels. Eur J Neurosci. 1995; 7:1527–1535. [PubMed: 7551179]

Nickells RW. Retinal ganglion cell death in glaucoma: the how, the why, the may be. J Glaucoma. 1996; 5:345–356. [PubMed: 8897235]

Ohira K, Shimizu K, Yamashita A, Hayashi M. Differential expression of the truncated TrkB receptor, T1, in the primary motor and prefrontal cortices of the adult macaque monkey. Neurosci Lett. 2005; 385(2):105–109. [PubMed: 15941622]

Oyesiku NM, Evans CO, Houston S, Darrell RS, Smith JS, Fulop ZL, Dixon CE, Stein DG. Regional changes in the expression of neurotrophic factors and their receptors following acute traumatic brain injury in the adult rat brain. Brain Res. 1999; 833:161–172. [PubMed: 10375691]

Parrilla-Reverter G, Agudo M, Sobrado-Calvo P, Salinas-Navarro M, Villegas-Perez MP, Vidal-Sanz M. Effects of different neurotrophic factors on the survival of retinal ganglion cells after a complete intraorbital nerve crush injury: a quantitative in vivo study. Exp Eye Res. 2009; 89:32–41. [PubMed: 19268467]

Pease ME, McKinnon SJ, Quigley HA, Kerrigan-Baumrind LA, Zack DJ. Obstructed axonal transport of BDNF and its receptor TrkB in experimental glaucoma. Invest Ophthalmol Vis Sci. 2000; 41:764–774. [PubMed: 10711692]

Quigley HA. Neuronal death in glaucoma. Prog Retin Eye Res. 1999; 18:39–57. [PubMed: 9920498]

Quigley HA, Broman AT. The number of people with glaucoma worldwide in 2010 and 2020. Br J Ophthalmol. 2006; 90:262–267. [PubMed: 16488940]

Quigley HA, McKinnon SJ, Zack DJ, Pease ME, Kerrigan-Baumrind LA, Kerrigan DF, Mitchell RS. Retrograde axonal transport of BDNF in retinal ganglion cells is blocked by acute IOP elevation in rats. Invest Ophthalmol Vis Sci. 2000; 41:3460–3466. [PubMed: 11006239]

Reichstein D, Ren L, Filippopoulos T, Mittag T, Danias J. Apoptotic retinal ganglion cell death in the DBA/2 mouse model of glaucoma. Exp Eye Res. 2007; 84:13–21. [PubMed: 17074320]

Sappington RM, Carlson BJ, Crish SD, Calkins DJ. The microbead occlusion model: a paradigm for induced ocular hypertension in rats and mice. Invest Ophthalmol Vis Sci. 2010; 51:207–216. [PubMed: 19850836]

Sappington RM, Sidorova T, Long DJ, Calkins DJ. TRPV1: contribution to retinal ganglion cell apoptosis and increased intracellular Ca2+ with exposure to hydrostatic pressure. Invest Ophthalmol Vis Sci. 2009; 50:717–728. [PubMed: 18952924]

Sasaoka M, Nakamura K, Shimazawa M, Ito Y, Araie M, Hara H. Changes in visual fields and lateral geniculate nucleus in monkey laser-induced high intraocular pressure model. Exp Eye Res. 2008; 86:770–782. [PubMed: 18378230]

Schlamp CL, Li Y, Dietz JA, Janssen KT, Nickells RW. Progressive ganglion cell loss and optic nerve degeneration in DBA/2J mice is variable and asymmetric. BMC Neurosci. 2006; 7:66. [PubMed: 17018142]

Schuettauf F, Rejdak R, Walski M, Frontczak-Baniewicz M, Voelker M, Blatsios G, Shinoda K, Zagorski Z, Zrenner E, Grieb P. Retinal neurodegeneration in the DBA/2J mouse-a model for ocular hypertension. Acta Neuropathol. 2004; 107:352–358. [PubMed: 14745571]

Song XY, Li F, Zhang FH, Zhong JH, Zhou XF. Peripherally-derived BDNF promotes regeneration of ascending sensory neurons after spinal cord injury. PLoS One. 2008; 3:e1707. [PubMed: 18320028]

Susanna R Jr. Unpredictability of glaucoma progression. Curr Med Res Opin. 2009; 25:2167–2177. [PubMed: 19601708]

Tanaka H, Ito Y, Nakamura S, Shimazawa M, Hara H. Involvement of brain-derived neurotrophic factor in time-dependent neurodegeneration in the murine superior colliculus after intravitreal injection of N-methyl-D-aspartate. Mol Vis. 2009; 15:662–669. [PubMed: 19347051]

Tongiorgi E, Armellin M, Giulianini PG, Bregola G, Zucchini S, Paradiso B, Steward O, Cattaneo A, Simonato M. Brain-derived neurotrophic factor mRNA and protein are targeted to discrete dendritic laminas by events that trigger epileptogenesis. J Neurosci. 2004; 24:6842–6852. [PubMed: 15282290]

Valverde F. The neuropil in superficial layers of the superior colliculus of the mouse. A correlated Golgi and electron microscopic study. Z Anat Entwicklungsgesch. 1973; 142:117–147. [PubMed: 4781860]

Weber AJ, Viswanathan S, Ramanathan C, Harman CD. Combined application of BDNF to the eye and brain enhances ganglion cell survival and function in the cat after optic nerve injury. Invest Ophthalmol Vis Sci. 2010; 51:327–334. [PubMed: 19710411]

Wilms P, Bahr M. Reactive changes in the adult rat superior colliculus after deafferentation. Restor Neurol Neurosci. 1995; 9:21–34. [PubMed: 21551831]

Yang J, Siao CJ, Nagappan G, Marinic T, Jing D, McGrath K, Chen ZY, Mark W, Tessarollo L, Lee FS, Lu B, Hempstead BL. Neuronal release of proBDNF. Nat Neurosci. 2009; 12:113–115. [PubMed: 19136973]

Yao PJ, Coleman PD, Calkins DJ. High-resolution localization of clathrin assembly protein AP180 in the presynaptic terminals of mammalian neurons. J Comp Neurol. 2002; 447:152–162. [PubMed: 11977118]

Yucel Y, Gupta N. Glaucoma of the brain: a disease model for the study of transsynaptic neural degeneration. Prog Brain Res. 2008; 173:465–478. [PubMed: 18929128]

Zhang S, Wang H, Lu Q, Qing G, Wang N, Wang Y, Li S, Yang D, Yan F. Detection of early neuron degeneration and accompanying glial responses in the visual pathway in a rat model of acute intraocular hypertension. Brain Res. 2009; 1303:131–143. [PubMed: 19765568]

Zhou X, Li F, Kong L, Tomita H, Li C, Cao W. Involvement of inflammation, degradation, and apoptosis in a mouse model of glaucoma. J Biol Chem. 2005; 280:31240–31248. [PubMed: 15985430]

Zuccato C, Cattaneo E. Role of brain-derived neurotrophic factor in Huntington's disease. Prog Neurobiol. 2007; 81:294–330. [PubMed: 17379385]

Zuccato C, Cattaneo E. Brain-derived neurotrophic factor in neurodegenerative diseases. Nat Rev Neurol. 2009; 5:311–322. [PubMed: 19498435]

HIGHLIGHTS

- Glaucoma involves degeneration of the retinal ganglion cell projection.
- Deficits in retinal axon transport to the superior colliculus (SC) are retinotopic.
- BDNF increases retinotopically in the SC with transport loss prior to synapse loss.
- Astrocytes become hypertrophic in the transport lesion.
- Astrocytes may sequester BDNF for focal re-release.

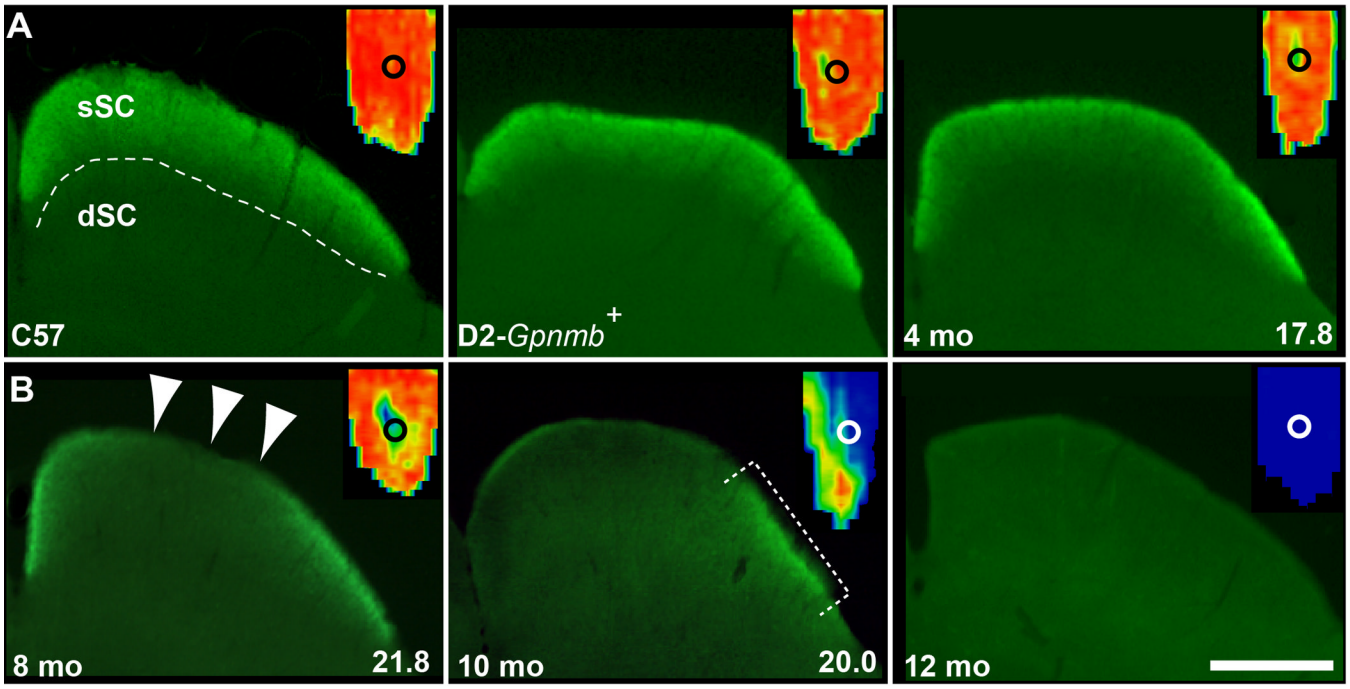

Figure 1.

Micrographs of the superior colliculus (SC) in cross-section (coronal plane) following intravitreal injections of cholera toxin β (CTB). A) SC of C57BL/6 (C57), D2-Gpnmb+, and a 4 mo DBA/2J each demonstrate intact CTB signal (green). Dashed line demarcates retinal recipient zone in superficial SC (sSC) from deep (dSC). B) SC from an 8 mo DBA/2J (left) shows a focal deficit (arrowheads), while a 10 mo (middle) has only residual signal (bracket) and a 12 mo (right) has complete depletion. Insets show retinotopic map reconstructed from serial sections through each SC with representation of optic disc gap (circle). Signal density ranges from 100% (red) to 50% (green) to 0% (blue) (Crish et al., 2010). Average lifetime IOP for the 4, 8 and 10 mo DBA/2J is indicated. Scale = 500 μm.

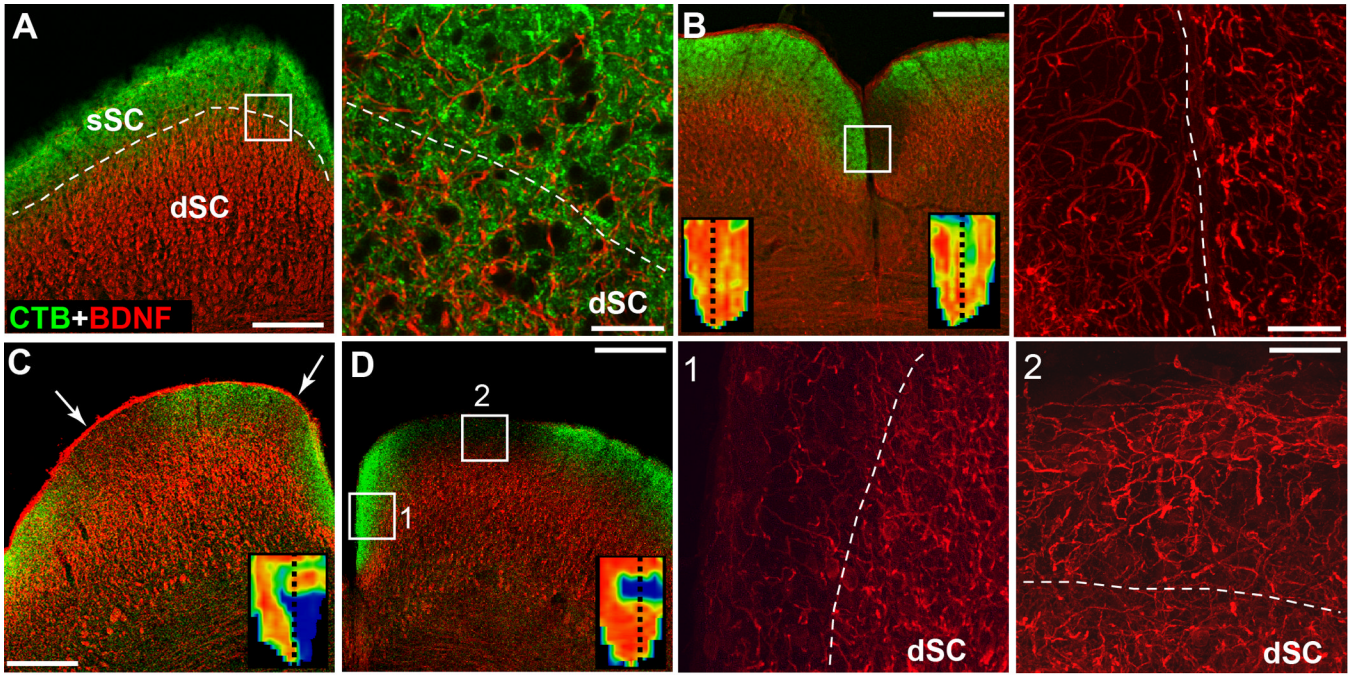

Figure 2. Focal elevation of BDNF with transport deficit

A) C57 SC demonstrates intact CTB transport and robust BDNF localization primarily in dSC (left panel). A higher-magnification view of boxed area (right panel) indicates little overlap. B) A 3 mo DBA/2J with a focal deficit in CTB signal in right SC (left panel). Boxed area (right) with CTB signal omitted shows clear BDNF elevation right of the midline (dashed line). C) Another 3 mo DBA/2J SC shows elevated BDNF within two focal deficits in CTB signal (arrows). D) An 8 mo DBA/2J SC demonstrates areas of intact (1) vs. depleted (2) CTB signal (left panel). High magnification of the two areas with CTB omitted (right) shows BDNF increasing in the second area above the dSC border with the sSC (dashed line).

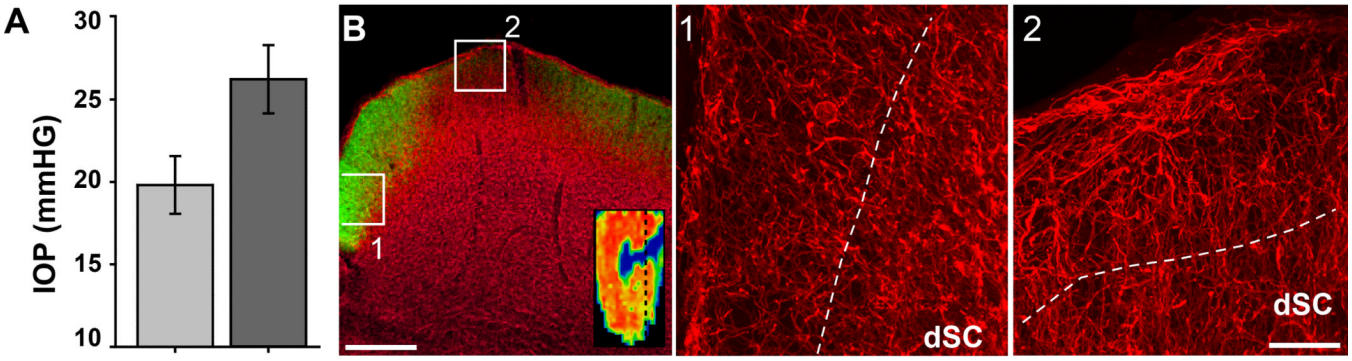

Figure 3. Focal elevation of BDNF with transport loss in an acute rat model

A) IOP of 26.2 ± 2.0 mmHG (mean ± sd) averaged over 5 weeks after microbead injection of a rat eye (dark bar) compared 19.8 ± 1.8 mmHG for an equal-volume saline injection in the opposing eye (light bar) for the same period ($p < 0.001$). B) The rat SC after IOP elevation shows regions with intact (1) vs. depleted (2) CTB signal (green, left panel). High magnification of the two areas shows increased BDNF (red) in the sSC of the second area (right panels). Inset shows corresponding retinotopic map with location of the coronal section (dotted line). Scale = 200 μm (low magnification panel) or 50 μm (high magnification panels).

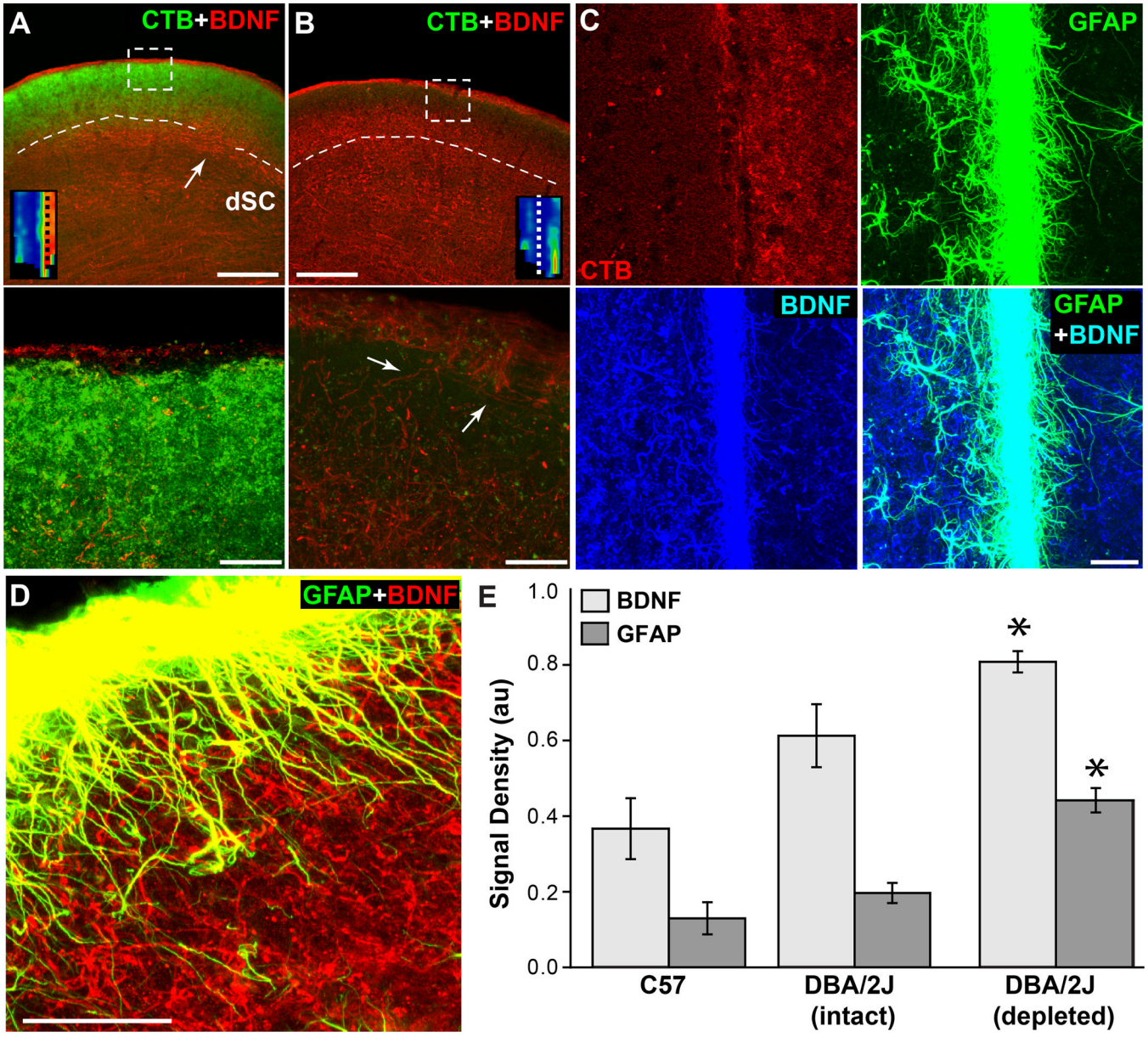

Figure 4. BDNF increases with astrocyte hypertrophy

A) Coronal section from a 10 mo DBA/2J SC shows mostly intact CTB signal in superficial layers and BDNF label primarily in dSC (top panel). BDNF is increased where transport is lower (arrow). Retinotopic map (inset) shows location of section (dotted line); only residual transport remains in SC. A higher-magnification view of boxed area (bottom panel) indicates very little BDNF overlap with CTB. Mean lifetime IOP = 17.6 mmHG. B) Section through another 10 mo DBA/2J SC with very little remaining CTB signal shows increased BDNF through superficial layers. High magnification of boxed region shows BDNF in astrocyte-like processes (bottom panel). IOP = 18.5. C) High magnification view of the midline between the two SC from a 10 mo DBA/2J shows unilateral loss of CTB signal in left SC (left panel) with coincident hypertrophy of GFAP-labelled astrocyte processes (right panel). BDNF increases with loss of CTB signal in left SC and co-localizes with astrocytes (bottom panels). Mean IOP = 17.7 and 16.7, respectively. D) Dorsal ridge of 10 mo SC with depleted CTB signal shown in (C) with BDNF-expressing astrocytes encroaching the RGC

recipient zone. E) Comparison of GFAP and BDNF signal between C57 SC, regions of DBA/2J SC with intact CTB signal, and regions with depleted CTB (mean ± sd). With depleted transport, both BDNF and GFAP increased compared to C57 SC and to intact DBA/2J SC (* indicates $p<0.001$ for BDNF and GFAP compared to C57; $p= 0.027$ for BDNF and $p<0.001$ for GFAP compared to DBA/2J intact). Scale = 200 μm (A and B, top panels) or 50 μm (C and D).

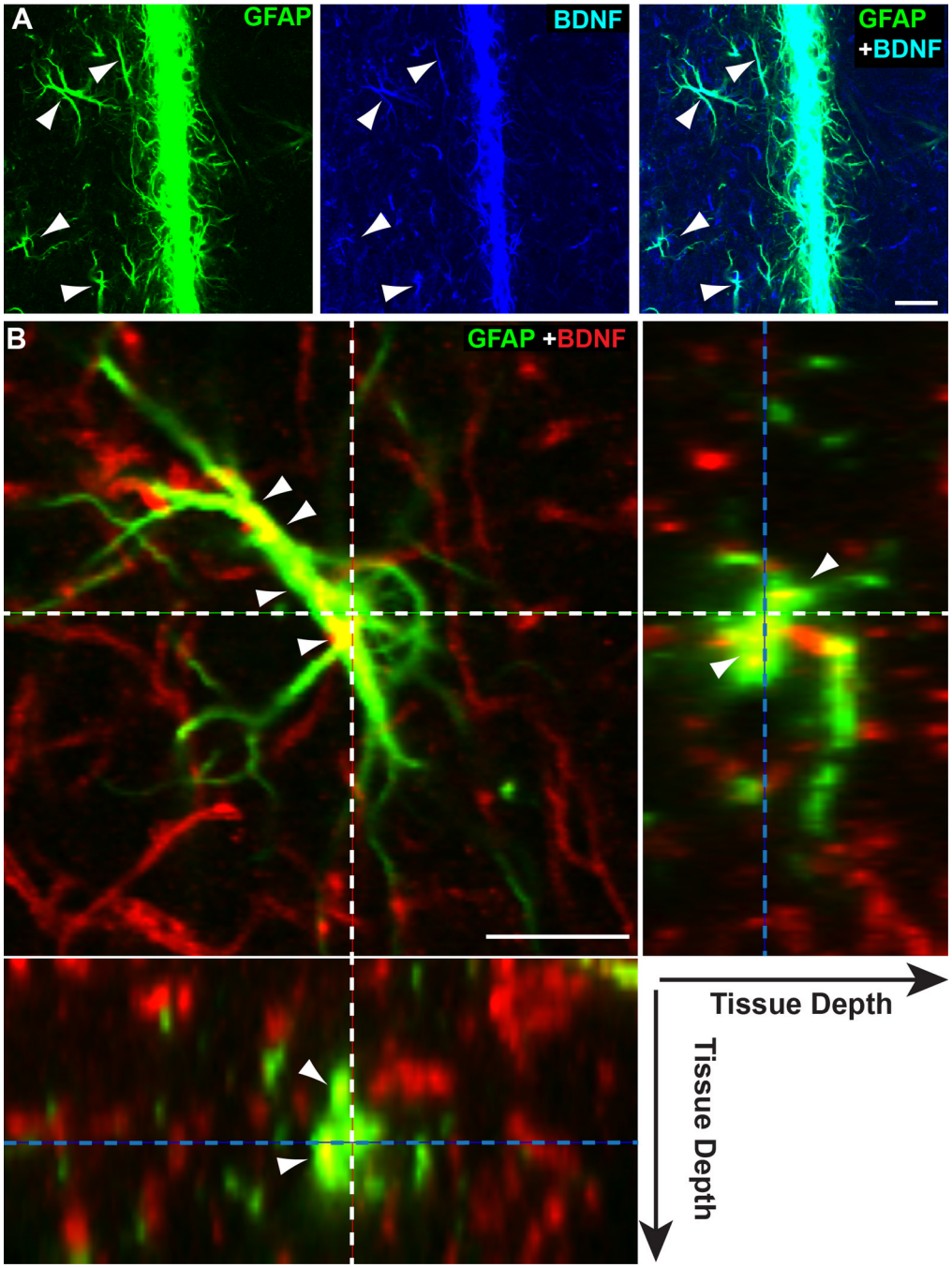

Figure 5. Localization of BDNF within astrocytes

A) High magnification of single-plane (1.5 μm thick) through the midline between the two SC from the 10 mo DBA/2J shown in Figure 4C. Image shows apparent localization of BDNF within GFAP-labelled hypertrophic astrocyte processes (arrowheads). B) Single-plane (1.5 μm thick) image of a GFAP-labelled astrocyte near the dorsal ridge of an 8 mo DBA/2J SC (left panel). End-on (orthogonal) view of the same plane for both the Y (right panel) and X (left panel) axes illustrates location in tissue of the image plane (dotted blue lines) and of center of the astrocyte (dotted white lines). While most BDNF distributes in the underlying neuropil, localization within the astrocyte forms diffusely distributed pockets within the cytoplasm (arrowheads). Smaller astrocyte processes, possibly end-feet, that are

associated with neuronal processes appear to contain far less BDNF. Scale = 20 μm (A) or 10 μm (B).

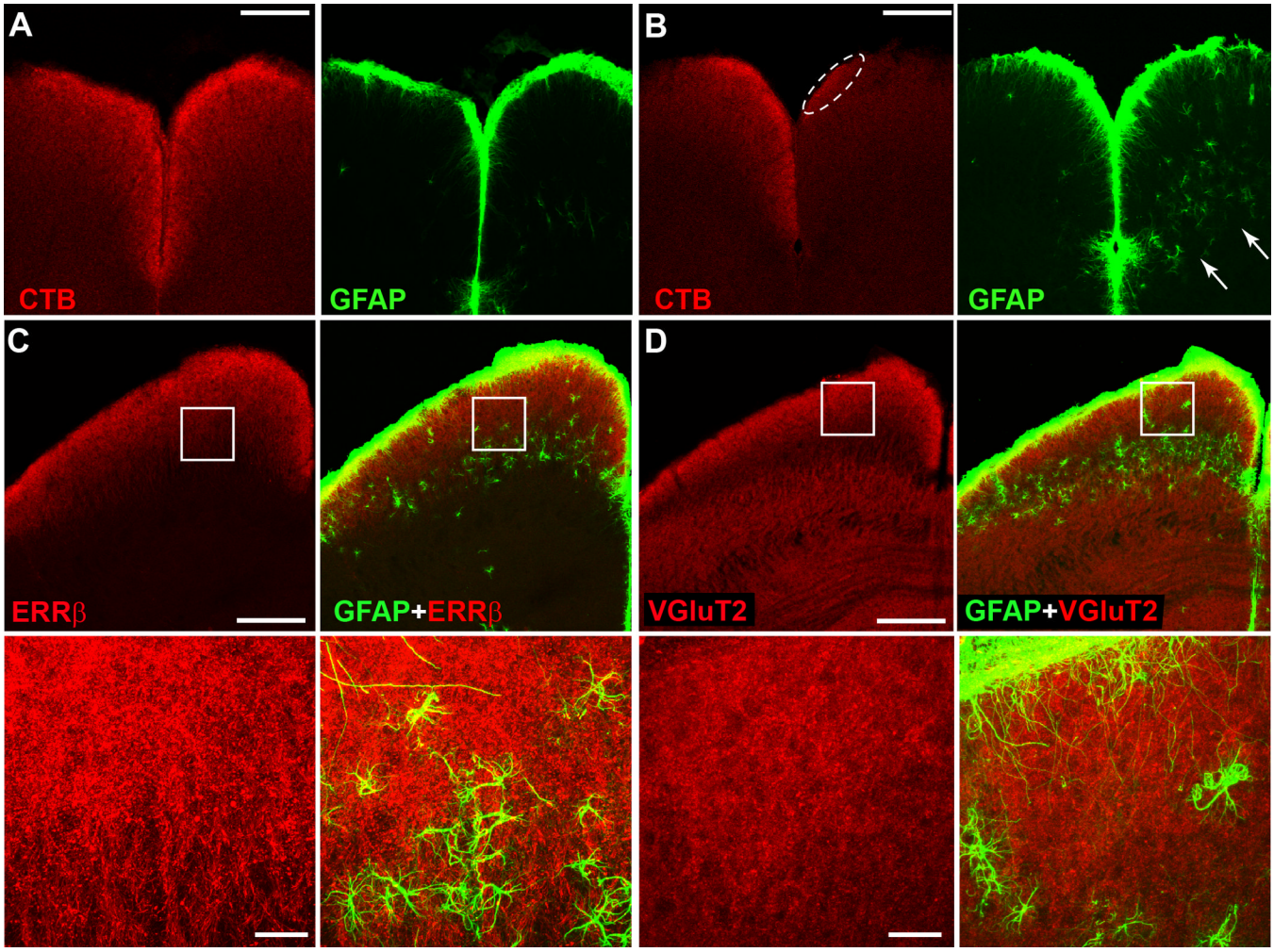

Figure 6. Astrocyte hypertrophy accompanies transport depletion and precedes structural loss

A) An 8 mo DBA/2J demonstrates intact CTB transport in both SC with modest GFAP label along the midline and dorsal ridge (right panel). B) Another 8 mo DBA/2J with intact CTB in one SC and only residual signal in the other (circled). With loss of CTB signal, GFAP-labelled astrocytes become hypertrophic throughout the SC (arrows). C, D) Two 10 mo DBA/2J SCs with completely depleted CTB signal (not shown) demonstrate persistence of the RGC axonal projection marker estrogen-related receptor beta (ERRβ, C) and RGC axon terminal marker vesicular glutamate transporter 2 (VGluT2, D). Both SC contain hypertrophic GFAP-labelled astrocytes (right panels). For both, boxed areas of higher magnification (bottom panels) show hypertrophic astrocytes in the RGC-recipient zone. Hypertrophy is also apparent in deeper SC, as in (B). Scale = 200 μm (A, B and C, D top panels) or 25 μm (C, D, bottom panels).

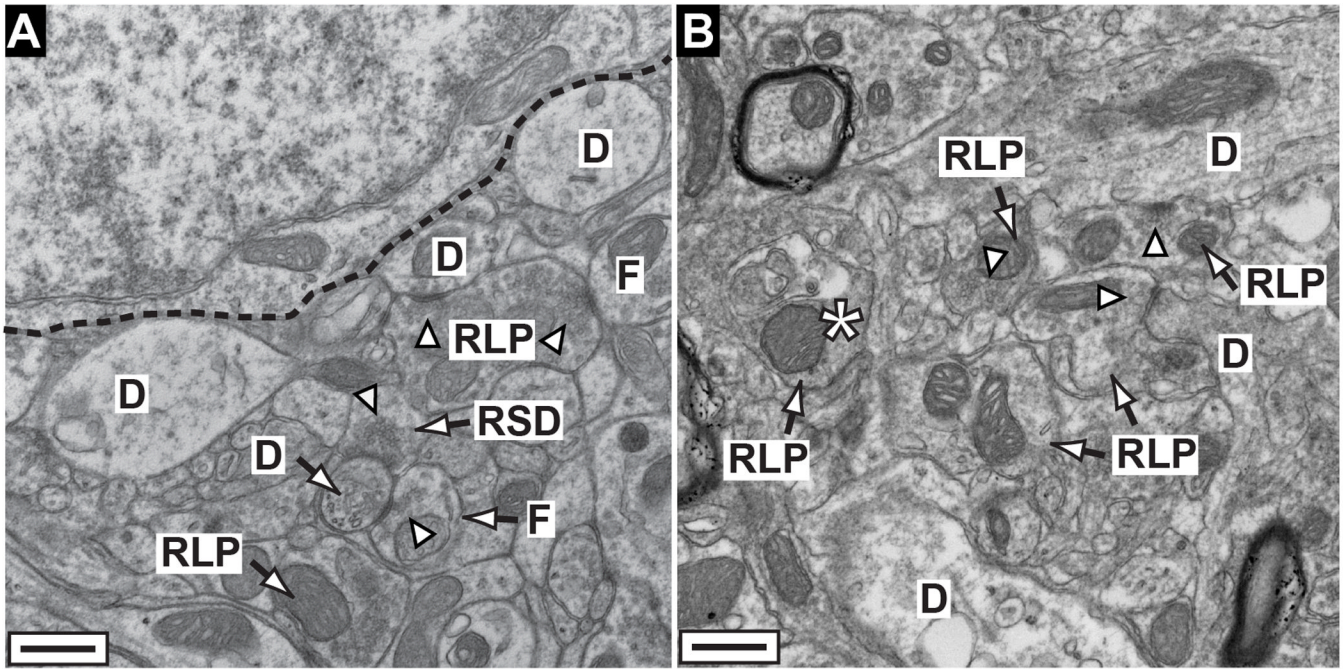

Figure 7. Structural persistence following transport depletion

A) Electron micrograph of sagittal section through superficial SC from a 12 mo DBA/2J shows axon terminals from RGCs (RLP), intracollicular inhibitory neurons (F), and cortico-collicular projections (RSD) in proximity to a collicular relay neuron (dashed line) and dendrites (D). For definitions, see Calkins et al. (Calkins et al., 2005). Many terminals contain intact presynaptic active zones (arrowheads). B) A 15 mo DBA/2J colliculus also contains intact RLP terminals with some synapses to dendrites. Terminals near a degenerating RLP (*) appear slightly dystrophic.

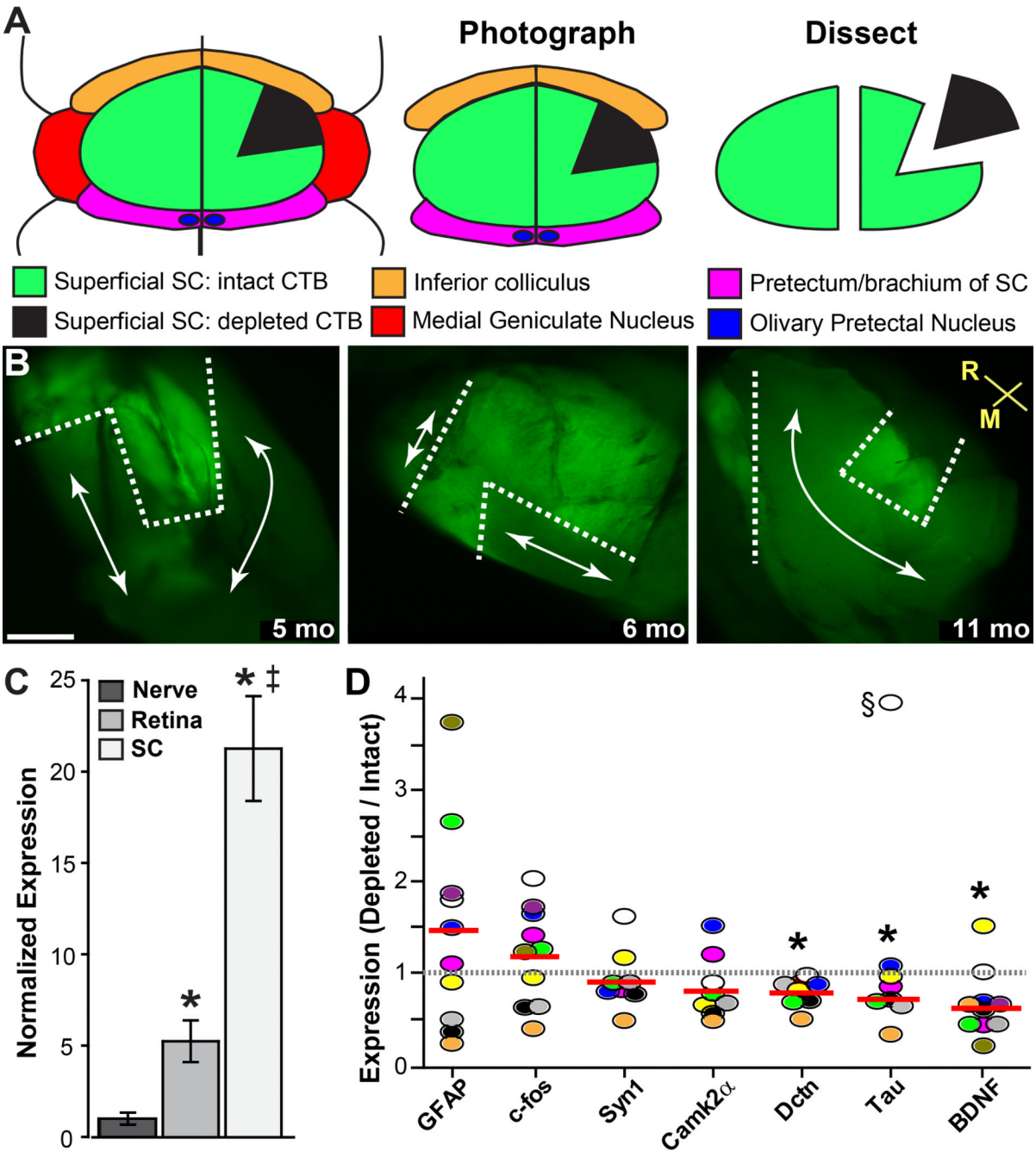

Figure 8. Gene expression with loss of transport in DBA/2J superior colliculus

A) Schematic of a mouse brain in horizontal section showing orientation of the superficial superior colliculus (SC) in relation to other structures. The SC and surrounding tissue are isolated ex vivo, flat-mounted on a slide, and photographed. Finally, regions with intact CTB signal (green) and regions with depleted signal (black) are micro-dissected from each other and processed for RNA extraction. B) Representative fluorescent micrographs of three freshly-dissected and flattened DBA/2J SCs. For each, we isolated regions of intact (within dotted lines) and depleted (arrows) transport, followed by RNA extraction. Rostral and medial orientation indicated. Scale = 200 μm. C) Quantitative PCR measurements of Bdnf mRNA in retina, myelinated optic nerve, and super colliculus of 3 mo C57. For each of 5

animals, tissues from the left and right retinal projections were pooled. Data calculated relative to 18s rRNA and normalized to expression in the nerve (mean ± sd). Compared to Bdnf mRNA in the optic nerve, expression in retina was 5-fold more abundant and in SC 21-fold more abundant (*; $p<0.001$). SC was 4-fold greater than retina (‡; $p<0.001$). D) Quantitative PCR measurements of select genes in 10 individual SCs (circles) shown as ratio of expression in region of depleted to intact transport, with mean ratio for each gene indicated (red line). For each micro-dissected region, expression was performed in triplicate and normalized to 18s rRNA before calculating the ratio. Significance: * $p=0.0004$ (Dctn), $p=0.017$ (Tau), and $p=0.008$ (Bdnf) compared to hypothetical ratio of one (dotted line) using chi-square. Outlier excluded (§, $p<0.001$).

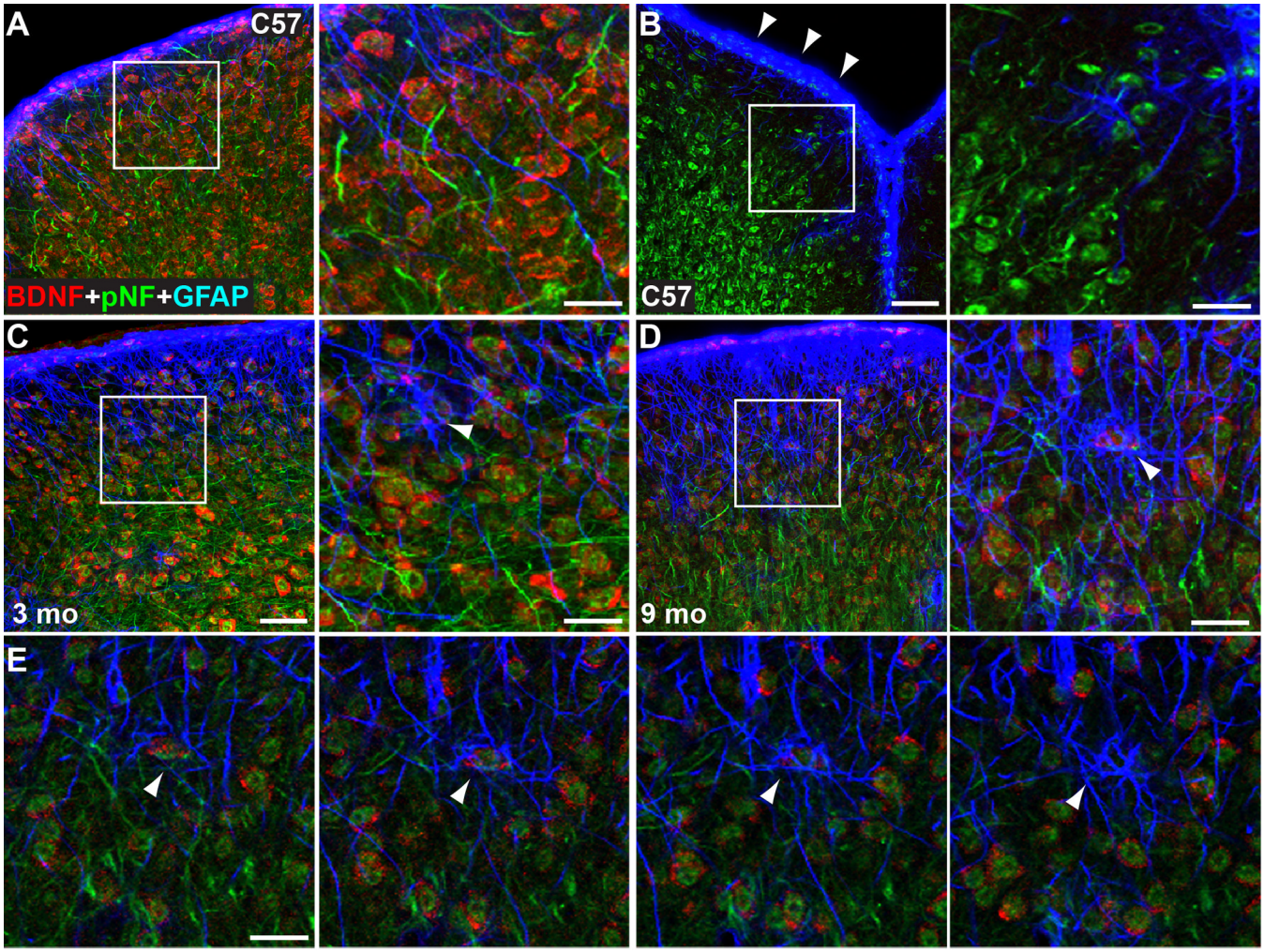

Figure 9. Bdnf mRNA in superior colliculus

A) *Bdnf* antisense probe (red) heavily labelled collicular neurons expressing phosphorylated neurofilament (pNF, green) in the C57 colliculus. GFAP-expressing astrocytes (blue) lying adjacent to pNF+ neurons along the dorsal border of superficial layer 1 also appeared to express *Bdnf*. A higher-magnification view of the boxed area indicates intense co-localization of *Bdnf* and pNF. B) Control *Bdnf* sense probe (red) elicits no label, as expected, in stacked images through C57 colliculus. pNF+ cell bodies along border (arrowheads) are sheathed with astrocyte processes. C) A 3 mo DBA/2J colliculus demonstrates increased GFAP and similar pattern of *Bdnf*. GFAP+ processes with *Bdnf* are less prominent than neuronal expression in the deeper layers of the superficial SC (arrowhead). (D) *Bdnf* expression decreases in 9 mo DBA/2J colliculus with increased GFAP in astrocytes. Higher magnification shows confluence of astrocyte processes overlying *Bdnf*-expressing neuron (arrowhead). Images in A–D are stacked confocal planes. (E) Series of single plane images through colliculus shown in (D) illustrates astrocyte processes enveloping a *Bdnf*-expressing neuron (arrowheads). Scale = 50 μm (low magnification panels) or 20 μm (high magnification).

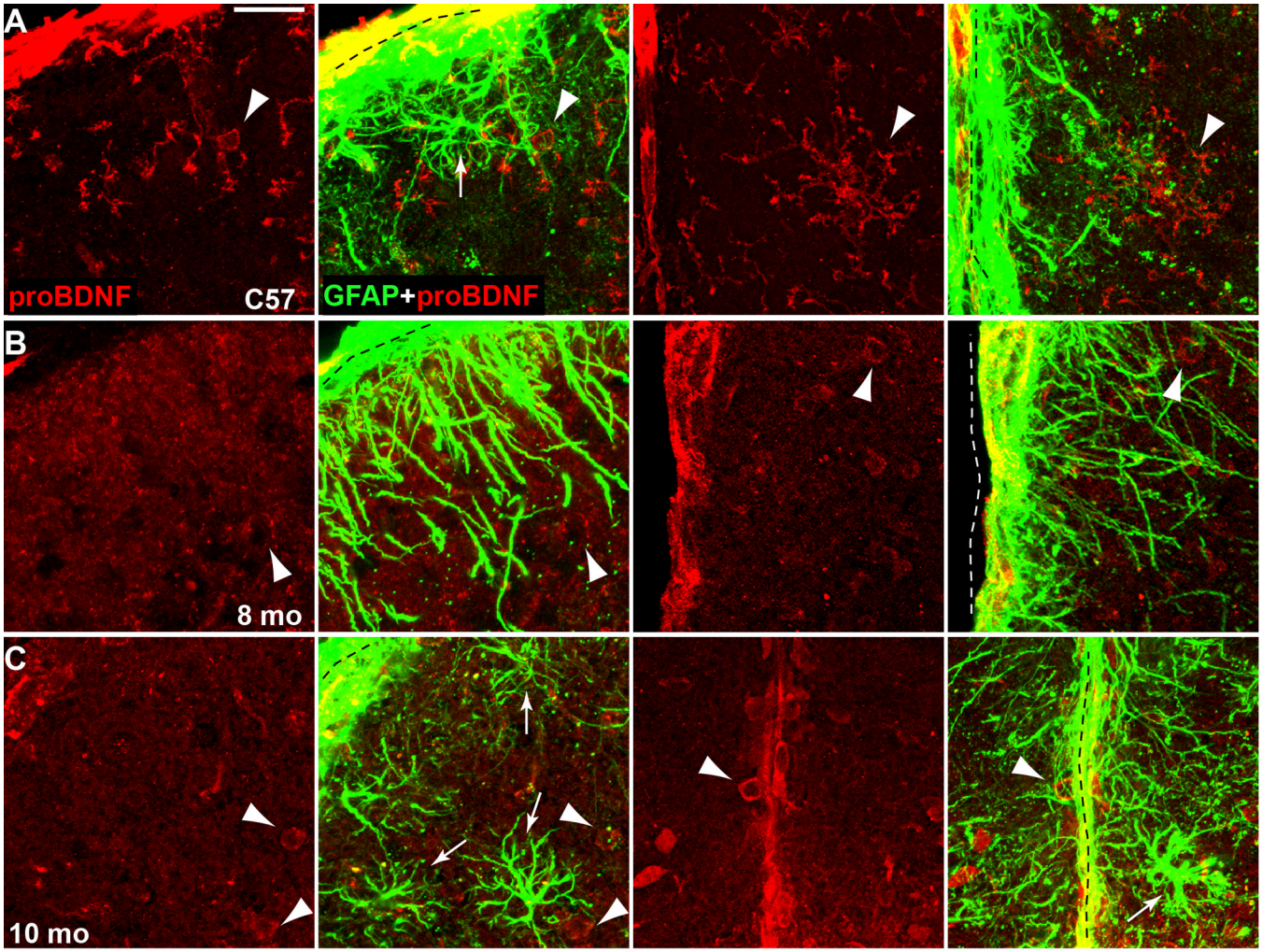

Figure 10. pro-BDNF localization in superior colliculus

A) Coronal section of C57 SC immuno-labelled for pro-BDNF shows modest signal in cells resembling microglia (arrowheads) and very little in GFAP-labelled astrocytes (arrow), both near the dorsal ridge of the SC (left panels) and SC midline (right panels). B) SC of 8 mo DBA/2J also shows little co-localization of pro-BDNF and GFAP, both at dorsal (left panels) and lateral (right panels) ridges. Pro-BDNF signal is most prominent in small cell bodies (arrowheads). C) For 10 mo DBA/2J SC, both at dorsal ridge (left) and midline (right), pro-BDNF signal is highest in small cells (arrowheads) and absent from GFAP-labelled astrocytes (arrows). For all samples, co-localization of pro-BDNF and GFAP was restricted to the borders of the SC (dotted lines). Scale = 20 μm for all panels.

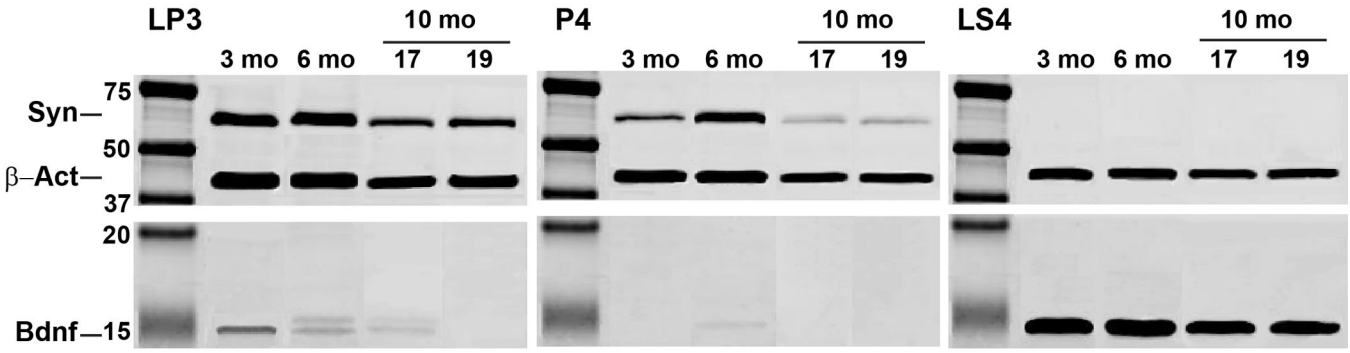

Figure 11. Subcellular detection of BDNF in superior colliculus

Western blot detection of BDNF in subcellular fractions of superior colliculus from 3, 6 and two sets of 10 month DBA/2J mice; three independent samples were pooled for each set. Mean IOP is indicated for the 10 month sets and was 15.7 for the 6 month samples. Detection of the synaptic vesicle membrane protein synaptotagmin (~65 kDa) was strongest in the light-membrane synaptosomal pellet (LP3), present but weaker in the high-speed vesicle fraction (P4), especially at 10 mo, and absent as expected in the high-speed supernatant of released vesicle content (LS4). In contrast, BDNF (~14 kDa) was weak and decreased with age in the LP3 fraction, was absent in the P4 fraction, and highly concentrated in LS4. Detection of β-Actin (~45 kDa) was used as a positive control.